Modulation of flow, heat, and mass transfer in turbulent double-diffusive convection

KenjereS, S.; Roovers, R.

DOI
10.1088/1742-6596/2766/1/012006

Publication date
2024

Document Version
Final published version

Published in
Journal of Physics: Conference Series

Modulation of flow, heat, and mass transfer in turbulent double-diffusive convection

Journal of Physics: Conference Series **2766** (2024) 012006 doi:10.1088/1742-6596/2766/1/012006

Modulation of flow, heat, and mass transfer in turbulent double-diffusive convection

S. Kenjereš and R. Roovers

Department of Chemical Engineering, Faculty of Applied Sciences, Delft University of Technology, Van der Maasweg 9, 2629 HZ Delft, The Netherlands

E-mail: s.kenjeres@tudelft.nl

Abstract. The present study addresses numerical simulations of the double-diffusive convection in a turbulent regime. The characteristic concentration and temperature Prandtl numbers ($Pr_C = 700$ and $Pr_T = 7$) correspond to the typical seawater properties. Here, we applied the Large-Eddy Simulation (LES) approach, with relatively simple subgrid turbulence closures of momentum, concentration, and temperature for the unresolved scales. The wall-resolved LES approach proved to work well on significantly coarser numerical mesh than used in recent Direct Numerical Simulation (DNS) studies of Yang et al. (2016) in the intermediate range of working parameters, $10^7 \leq Ra_C \leq 10^9$, $0 \leq Ra_T \leq 10^6$, which covers the quasi-Rayleigh-Bénard, fingering, and damping flow regimes. A good agreement between concentration and temperature Nusselt numbers is obtained. The instantaneous Nusselt numbers distribution revealed a significant impact of the imposed strong thermal stratification ($Ra_T = 10^6$) in comparison to the neutral case ($Ra_T = 0$).

1. Introduction

The combined effects of the thermal and concentration buoyancy (double-diffusive convection) play an important role in various environmental (mixing in the upper layer of oceans), astrophysical (helium-core stars), and industrial (energy storage tanks) applications, [1], [2], [3], [4], [5]. In the present study, we focus on a situation typical for the ocean's upper layer where the concentration gradient is the main driving mechanism to initiate mixing, whereas the temperature gradient plays a suppressing role. Because of high values of characteristic Prandtl numbers (i.e. thermal $Pr_T = \mathcal{O}(10)$, and concentration $Pr_C = \mathcal{O}(10^2)$), in order to make numerical simulation costs acceptable, we adopt the wall-resolving Large-Eddy Simulation (LES) approach, [8], [9], [10], [11].

2. Governing equations

The transport of mass, momentum, heat and species in the double diffusive convection in a turbulent regime is defined by the following spatially-averaging transport equations used in the Large Eddy Simulation (LES) approach, and can be written as:

$$\frac{\partial u_i}{\partial x_i} = 0 \tag{1}$$

$$\frac{\partial u_i}{\partial t} + \frac{\partial (u_i u_j)}{\partial x_j} = -\frac{1}{\rho_0}\frac{\partial p}{\partial x_i} + \frac{\partial}{\partial x_j}\left[\nu\left(\frac{\partial u_i}{\partial x_j} + \frac{\partial u_j}{\partial x_i}\right) - \tau_{ij}\right] - g_i\left[\beta_T\left(\theta - \theta_0\right) + \beta_C\left(c - c_0\right)\right] \tag{2}$$

$$\frac{\partial c}{\partial t} + \frac{\partial (cu_j)}{\partial x_j} = \frac{\partial}{\partial x_j}\left(D_c \frac{\partial c}{\partial x_j} - \tau_{cj}\right) \tag{3}$$

$$\frac{\partial \theta}{\partial t} + \frac{\partial (\theta u_j)}{\partial x_j} = \frac{\partial}{\partial x_j}\left(D_\theta \frac{\partial \theta}{\partial x_j} - \tau_{\theta j}\right) \tag{4}$$

where ρ_0 is density of fluid at reference temperature (θ_0) and concentration (c_0), β_T is thermal expansion coefficient, β_C is concentration expansion coefficient, D_θ is molecular thermal diffusion, D_c is molecular concentration diffusion, and, finally, τ_{ij}, τ_{cj}, $\tau_{\theta j}$ are subgrid turbulent stress tensor, concentration flux, and thermal flux, respectively, that need to be modeled. In the present work, we adopt the subgrid closure of [6], who proved to work well for turbulent thermal convection, [10]:

$$\tau_{ij} = -\nu_t \left(\frac{\partial u_i}{\partial x_j} + \frac{\partial u_j}{\partial x_i}\right) + \frac{1}{3}\langle u_k^{'} u_k^{'} \rangle \delta_{ij} \tag{5}$$

$$\nu_t = c\sqrt{\frac{B_\beta}{\alpha_{ij}\alpha_{ij}}}, \alpha_{ij} = \frac{\partial u_i}{\partial x_j}, \beta_{ij} = \Delta_m^2 \alpha_{mi}\alpha_{mj}, B_\beta = \beta_{11}\beta_{22} - \beta_{12}^2 + \beta_{11}\beta_{33} - \beta_{13}^2 + \beta_{22}\beta_{33} - \beta_{23}^2 \tag{6}$$

with a model coefficient $c = 0.07$, and the control volume filter-length projections Δ_m. The subgrid turbulent concentration and heat fluxes are modeled by a simple-gradient diffusion hypothesis (SGDH):

$$\tau_{cj} = -\frac{\nu_t}{Pr_C^t}\frac{\partial c}{\partial x_j}, \tau_{\theta j} = -\frac{\nu_t}{Pr_T^t}\frac{\partial \theta}{\partial x_j}, \tag{7}$$

with the adopted values of the turbulent Prandtl numbers of $Pr_C^t = 0.7$ and $Pr_T^t = 0.4$. The double diffusion phenomena is determined by the following set of the characteristic non-dimensional parameters, Ra_C, Pr_C, Ra_T, Pr_T. Here, $Pr_C = 700$ and $Pr_T = 7$, which corresponds to the seawater properties. In the present work, we focus on an intermediate range of working parameters, i.e. $10^7 \leq Ra_C \leq 10^9$, and $Ra_T = 0, 10^3, 10^6$ (where $Ra_T = 0$ indicates passive scalar behaviour of temperature, whereas $Ra_T = 10^6$ indicates a strong stable thermal stratification level).

3. Numerical method

The discretised forms of above defined governing equations are solved by our in-house finite-volume code for general non-orthogonal structured geometries. The collocated grid arrangement is applied for all transport variables. The Cartesian vector and tensor components are introduced. The Rhie-Chow interpolation is employed to prevent decoupling between the pressure and velocity fields. The SIMPLE algorithm is used to solve the pressure field. The code is of the second-order overall accuracy. Both convective and diffusive terms of all transport equations are calculated by the central-differencing scheme (CDS). The fully implicit time integration is performed using the three-time-level scheme, [7], [8], [9], [10].

4. Geometry, boundary conditions and numerical mesh

We consider a simple rectangular computational domain with the $L : D : H = 2 : 2 : 1$ aspect ratio, where the upper surface was kept at a constant high temperature (θ_h) and concentration (c_h), whereas the lower surface was kept at constant low temperature (θ_c) and concentration (c_c). The gravity acts in the negative vertical direction ($g(0, 0, -1)$), so imposed concentration gradient will tend to promote mixing, and temperature gradient will tend to stabilize the flow. All vertical walls were treated as a free-slip for velocity and zero-gradient fluxes for temperature and concentration, respectively. To properly resolve steep concentration and temperature

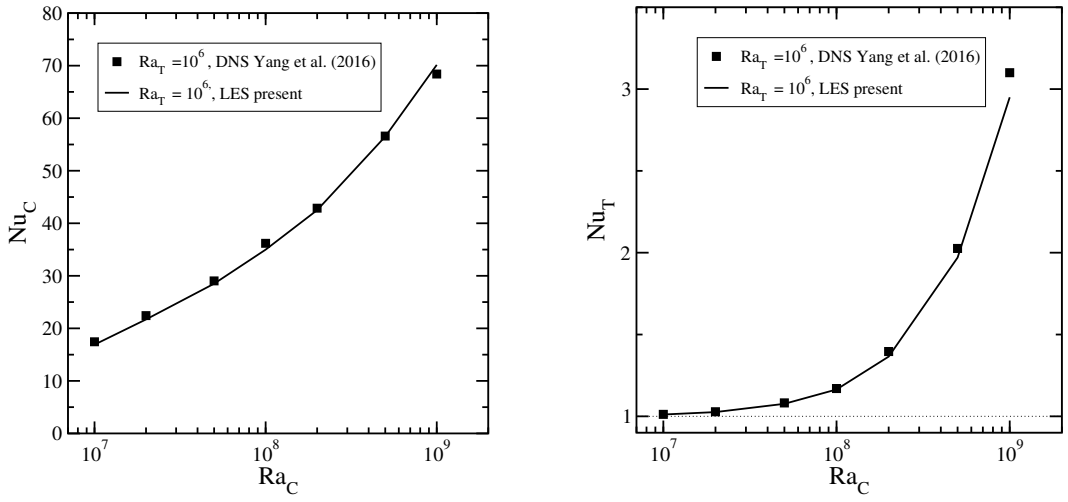

Figure 1. Comparative assessment of the integral Nusselt concentration (Nu_C) and temperature (Nu_T) numbers over a range of $10^7 \leq Ra_C \leq 10^9$ for a fixed value of $Ra_T = 10^6$.

gradients in the proximity of the horizontal walls, we apply a non-uniform mesh ($256 \times 256 \times 162$) such that concentration boundary layers are properly resolved (i.e. $\delta_c = 0.5HNu_C^{-1}$), and that we have an adequate resolution ($(5-10)\eta_B$) in the central part of domain to represent Batchelor scales (i.e. $\eta_B = \left(\nu^3/\varepsilon\right)^{1/4} / Pr_C^{1/2}$).

5. Results and discussion

We start our analysis by comparing the present LES results with DNS of [5], Fig.1. The DNS results of [5] were obtained with a dual mesh approach using 288^3 elements for the momentum and 864^3 elements for scalars, respectively. The present LES uses a single mesh of $256^2 \times 162$ control volumes for all transport variables. It can be seen that a very good agreement was obtained for both integral Nusselt numbers for concentration and temperature, over the entire range of Ra_C. There is a small deviation in the prediction of the Nu_T at $Ra_C = 10^9$ ($\Delta Nu_T = 4\%$). This can be explained by (i) changes in the aspect ratio of DNS, where the reduced geometry (1:1:0.8) was simulated, whereas we kept the original (2:2:1) ratio in all simulations, and (ii) significantly longer intervals of collecting statistics in our LES (10 times longer) compared to DNS. Contours of the instantaneous local Nusselt numbers at the upper boundary for $Ra_C = 10^7$ and two values of $Ra_T = 0$ and 10^6, are shown in Fig.2. It can be seen that for a strong thermal stratification case, both Nusselt numbers exhibit significantly smaller structures, confirming a reduction of mixing in the horizontal directions. Furthermore, the network of the concentration Nusselt number shows distinct polyhedral structures, whereas the temperature Nusselt number exhibits dominant circular imprints. Finally, the various values of Ra_T do not have a significant effect on the intensity of the local Nu_C, while the significantly stronger suppression is obtained for Nu_T. To understand observed distributions of the Nusselt numbers, we focus on analysis of the flow and scalar fields. The instantaneous streamlines in the central vertical plane for $Ra_C = 10^7$ and $Ra_T = 0$ and 10^6 are shown in Fig.3. It can be seen that the flow structures are suppressed in the horizontal direction at $Ra = 10^6$, forming a larger number of rolls. The local impinging points are locations where the local Nusselt numbers have their local maxima values, which explains the local similarity between the concentration and temperature Nusselt numbers. It can be seen that the eddy structures are reduced in the horizontal direction for a strong thermal stratification $Ra_T = 10^6$. Finally, contours of the instantaneous concentration at three characteristic horizontal planes ($z/H = 0.9, 0.5$, and 0.1)

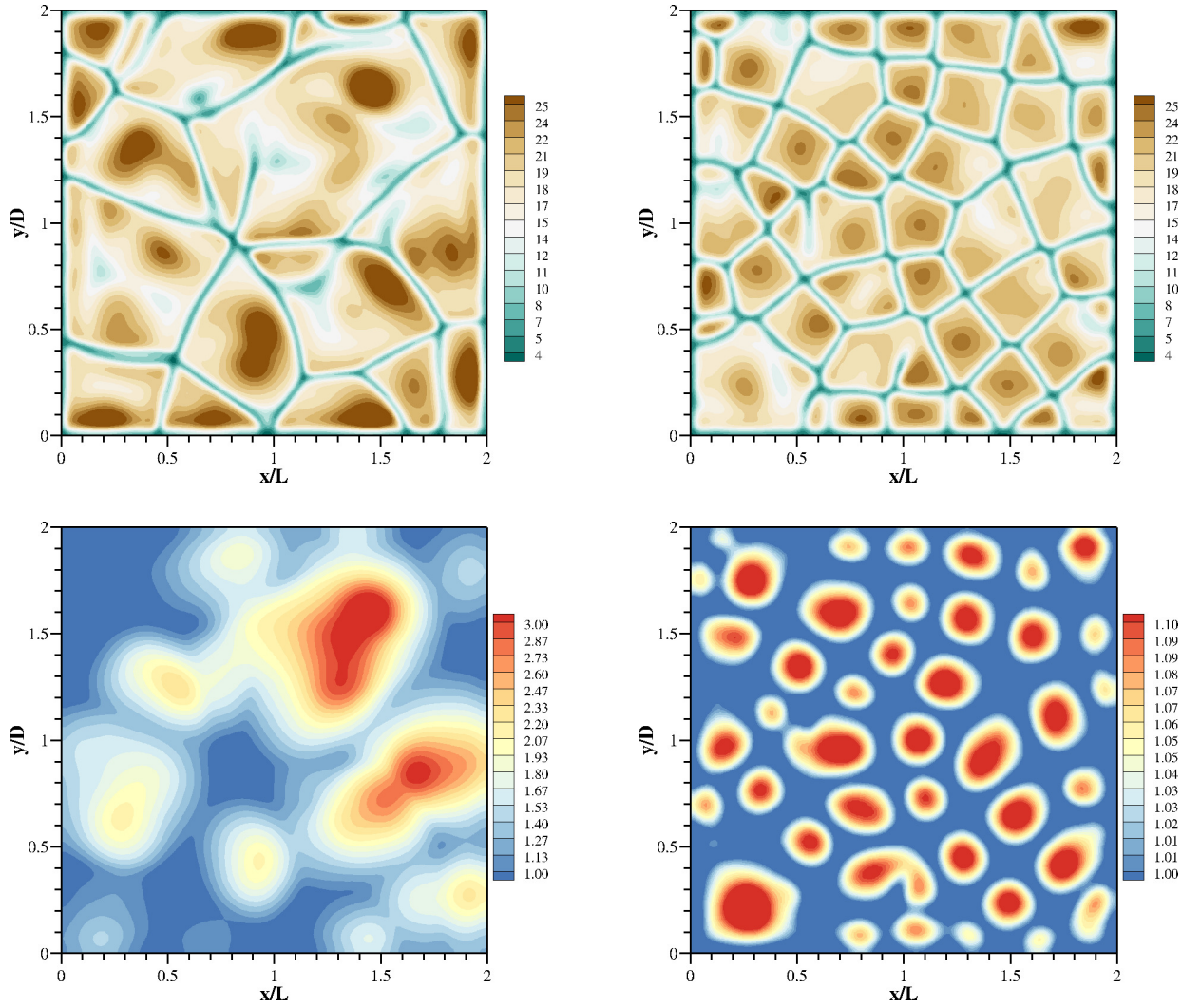

Figure 2. Contours of the instantaneous local concentration (Nu_C) (-top) and temperature (Nu_T) (-bottom) Nusselt numbers in the proximity of the upper boundary, $Ra_C = 10^7$, $Ra_T = 0$ (-left), $Ra_T = 10^6$ (-right).

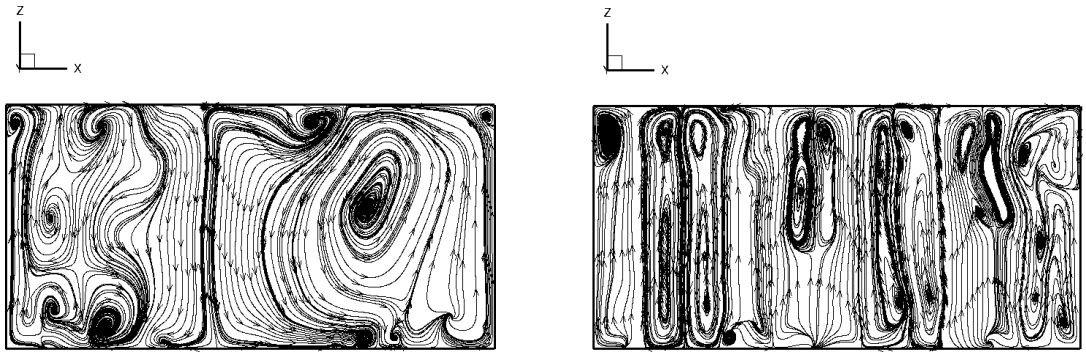

Figure 3. Instantaneous streamlines in the central vertical plane y/W=1, at $Ra_C = 10^7$, $Ra_T = 0$ (-left), $Ra_T = 10^6$ (right).

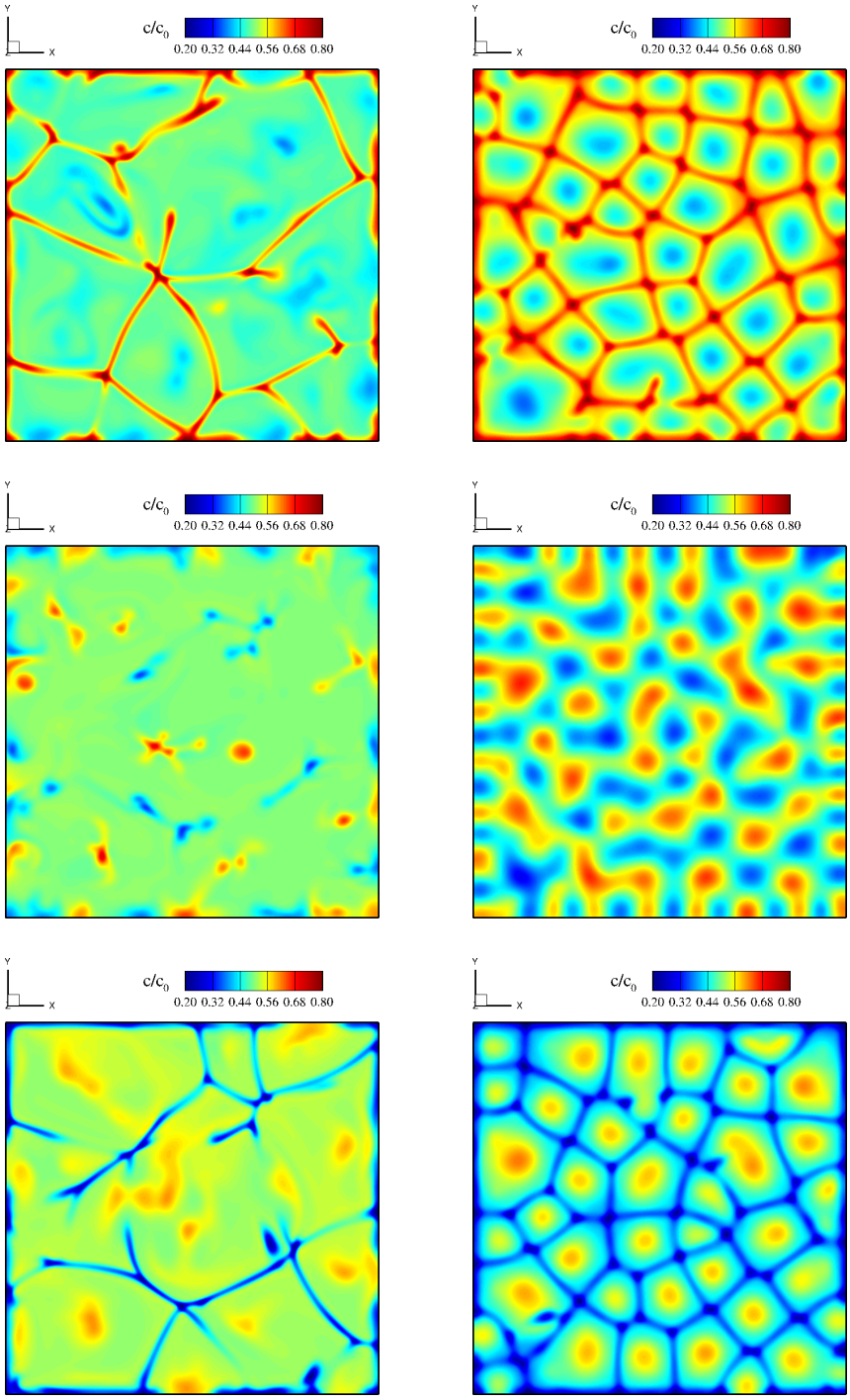

Figure 4. Contours of the instantaneous non-dimensional concentration (c/c_0, $c_0 = 0.5(c_h+c_c)$), at three characteristic locations: $z/H = 0.9$ (-top), $z/H = 0.6$ (-middle), $z/H = 0.9$ (-bottom), at $Ra_c = 10^7$, $Ra_T = 0$ (-left), $Ra_T = 10^6$ (-right).

are shown in Fig.4. In the proximity of the upper wall, characteristic planform structures with distinct thin boundaries can be observed at $Ra_T = 0$, Fig.4-top. In contrast, at $Ra_T = 10^6$, a significantly larger number of polyhedral structures is formed, with thicker boundaries. In the middle plane, there are isolated imprints of the concentration plumes (red-downdrafts,

blue-updrafts), which are significantly stronger at $Ra_T = 10^6$, Fig.4-middle. Finally, in the proximity of the bottom wall, we have an inverse behavior in comparison to the top wall. Again, distinct planform structures are present, but now with light concentration levels at the planform structures, and a heavy concentration imprints in the center.

6. Conclusions

In the present study, we demonstrated that the application of a wall-resolving Large-Eddy Simulation of the turbulent double-diffusive convection (DDC) with a simple sub-grid closure for the unresolved turbulent transport of the concentration and temperature fields, can be a good alternative to a much more computationally demanding Direct Numerical Simulations (DNS), especially for large values of the Prandtl numbers. This is confirmed by comparing the results of the present LES and DNS of [5] for integral values of the Nusselt concentration and temperature numbers in the intermediate range of $10^7 \leq Ra_C \leq 10^9$ and $0 \leq Ra_T \leq 10^6$, and fixed values of $Pr_C = 700$, and $Pr_T = 7$, which correspond to the seawater properties. The obtained results indicated a strong modulation of the flow, heat, and mass transfer for different strengths of the imposed thermal stratification.

References

[1] Turner J S 1974 *Annual Review of Fluid Mechanics* **6**, 37-56
[2] Turner J S 1985 *Annual Review of Fluid Mechanics* **17**, 11-44
[3] Zaussinger F, Kupka F 2019 *Theoretical and Computational Fluid Dynamics* **33**, 383–409
[4] Yang Y, Verzicco R, Lohse D 2016 *PNAS* **113** (1), 69–73
[5] Yang Y, Verzicco R, Lohse D 2016 *J. Fluid Mech.* **802**, 667-689
[6] Vreman A W 2004 *Phys. Fluids* **16**, 3670–3681
[7] Kenjereš S, Hanjalić K 2006 *Int. J. Heat and Fluid Flow* **27** (5), 800–810
[8] Kenjereš S 2008 *Phys. Rev. E* **78** 066309, 1–5
[9] Kenjereš S 2011 *Phys. Fluids* **21** 015103, 1–11
[10] Kenjereš S 2015 *Phys. Rev. E* **92** (5), 053006, 1–14
[11] Zenklusen A, Kenjereš S, Rudolf von Rohr P. 2016 *Chemical Engineering Science* **150**, 74–84